IR spectroscopy of the low-frequency phonon spectrum of the $TbFe_3(BO_3)_4$ single-crystal

Cite as: Low Temp. Phys. **40**, 1087 (2014); https://doi.org/10.1063/1.4904002
Published Online: 05 January 2015

V. S. Kurnosov, V. V. Tsapenko, L. N. Bezmaternykh, and I. A. Gudim

LOW-TEMPERATURE OPTICAL SPECTROSCOPY

IR spectroscopy of the low-frequency phonon spectrum of the $TbFe_3(BO_3)_4$ single-crystal

V. S. Kurnosov[a] and V. V. Tsapenko

B. Verkin Institute of Low Temperature Physics and Engineering of the National Academy of Sciences of Ukraine, 47 Lenin Ave., Kharkov 61103, Ukraine

L. N. Bezmaternykh and I. A. Gudim

L. Kirensky Physics Institute, Siberian Branch of the Russian Academy of Sciences, Krasnoyarsk 660036, Russia

(Submitted May 22, 2014; revised June 18, 2014)
Fiz. Nizk. Temp. **40**, 1397–1408 (December 2014)

A study of the IR reflectance spectra of the $TbFe_3(BO_3)_4$ crystal. We determined the frequencies of the polar lattice phonons in the high-temperature $R32$, and low- temperature $P3_121$, phases. All $8A_2 \oplus 11E$-modes were found in the high-temperature phase, with nine of them corresponding to lines of the absorption spectrum. In the low-temperature phase, of the $20A_2 \oplus 35E$-modes allowed by the symmetry of the crystal lattice, $20A_2 \oplus 25E$-modes were found. © *2014 AIP Publishing LLC*.
[http://dx.doi.org/10.1063/1.4904002]

Introduction

Interest in the family of ferroborates $ReFe_2(BO_3)_4$ (Re = Y, La-Nd, Sm-Ho) is caused by the peculiarities of their magnetic structure, which is caused by the rare-earth ion. The interaction of the latter with the iron ions has a significant effect on the magnetic anisotropy, and, as a result, on the orientation of the magnetic moments of the iron in relation to the crystallographic axes.[1,2]

All ferroborates experience antiferromagnetic ordering of the iron subsystem at temperatures ranging from 28 to 41 K.[3] During this process, some representatives of the family such as Pr, Tb, and Dy, acquire an easy-axis magnetic structure, whereas others, such as Nd, Sm, Eu, and Y, acquire an easy-plane. The magnetic reorientations are fixed for the Gd and Ho ferroborates at low temperatures, as a result of which the easy-axis state is replaced by easy-plane.[2] Some representatives of the ferroborates are multiferroic.[4]

For trivalent lanthanides, a decrease in their ionic radius is typical, as their atomic number increases. Therefore, the instability of the high-temperature rhombohedral $R32$ phase, is tied to the decrease of the rare-earth ionic radius in ferroborates, with the symmetry of this phase decreasing until $P3_121$, via a weak first-order structural phase transition (WPT), starting with the compounds containing Eu.[1–3]

A large number of studies are dedicated mainly to the magnetic and electric properties of ferroborates. A significantly smaller portion is dedicated to studies of the dynamics of the crystal lattice, even though the low-frequency polar vibrational excitations make a significant contribution to the dielectric properties of the medium. The data of only a few Raman measurements are known.[5–7] Raman scattering in a lattice polarizability is prohibited by the polar phonons, transformed according to the A_2 irreducible representation, factor-group 32 (D_3). Data about them, and also about the dipole modes of the E-symmetry, can be obtained directly from the infrared (IR) reflection spectroscopy.

Experimental procedure and samples

The $TbFe_3(BO_3)_4$ single-crystals, used for the preparation of test samples, were grown from a molten solution based on bismuth trimolybdate, according to the methodology described in Ref. 8.

Measurements of the IR reflectance spectra were conducted on two samples, cut from the $TbFe_3(BO_3)_4$ single-crystals. One of the samples was used for Raman scattering[5] and had the dimensions $2.2 \times 2.7 \times 4.8$ mm (sample No. 1). It was used for measuring the reflectance spectra, in which the wave vector $\mathbf{k}$ of the incident light is parallel to the optical axis of the crystal. The reflectance spectrum of this sample contains bands formed only by doubly-degenerate polar symmetry E-modes. The second sample was a plane-parallel mechanically polished plate, with a thickness of 1.45 mm, in which the optical axis of the crystal was parallel to the forming planes (sample No. 2). The reflectance spectrum of this sample in an unpolarized light is a superimposition of two components, formed by the polar symmetry E- and A_2-modes.

The spectra were recorded in a frequency range of 20–600 cm^{-1} using the LAFS-1000 Fourier spectrometer. The measurements were done in a cryostat in vacuum. The samples were mounted on a copper cold finger with a system of thermostabilization and thermometry, allowing for a constant temperature with an accuracy of no less than 0.5 K.

In order to analyze the experimental reflectance spectra, we calculated the reflectance of the crystal plane-parallel plate, the optical properties of which are described by the complex dielectric functions $\varepsilon_{||}(\omega)$ and $\varepsilon_{\perp}(\omega)$. The parallel and perpendicular signs correspond to the dielectric response of the uniaxial crystal to the external alternating electric field with the frequency ω, both along with, and perpendicular to, the trigonal axis, respectively. The reflection coefficient R, at a normal incidence to the plate, which is located above the surface of the metal mirror (this is the exact situation in the measurement cell), is described by the expression

$$R = \frac{R_d(1 + R_d R_m) + \lambda^4(R_d + R_m)}{(1 + R_d R_m) + R_d \lambda^4 (R_d + R_m)}, \quad (1)$$

where R_d is the reflection coefficient of a semi-infinite dielectric medium, R_m is the reflection coefficient of the metal mirror, and λ is the damping parameter of the electromagnetic wave in the dielectric layer. Expression (1) is derived using solutions of the Maxwell equations for plane waves, propagating perpendicularly to the plane-parallel interfaces of the media.[9] The oscillating terms, which occur as a result of interference, are excluded in the numerator and denominator. The formula is closest to the exact solution at a mirror reflectivity of $R_m \approx 1$ or $R_m \equiv 0$, which is a case of reflection from a single dielectric layer. The parameters included in expression (1) are expressed though the dielectric function in the following way:

$$r_d = -\frac{\eta - 1 + i\kappa}{\eta + 1 + i\kappa}, \quad R_d = |r_d|^2 = \frac{\eta^2 + \kappa^2 + 1 - 2\eta}{\eta^2 + \kappa^2 + 1 + 2\eta},$$
$$(\eta + i\kappa)^2 = \varepsilon(\omega), \quad \lambda = \exp(-\kappa d\omega/c),$$

where r_d is the amplitude reflection coefficient of the semi-infinite medium, η and κ are the real and imaginary parts of the refractive index at the frequency ω, d is the medium thickness, and c is the velocity of light in vacuum.

The $\varepsilon_\alpha(\omega)$ ($\alpha = \perp, ||$) themselves were expressed by the four-parameter factored Lyddane-Sachs-Teller (LST) model, following the authors of Refs. 10 and 11. This representation of the dielectric function is borrowed from Refs. 12–14, in which the optical properties of simple ionic crystals are examined. In contrast to the Drude-Lorentz model, where the dielectric function is the result of the summation of independent oscillators, LST has a multiplicative representation:

$$\varepsilon(\omega) = \varepsilon_\infty \prod_{j=1}^{N} \frac{\omega_{Lj}^2 - \omega^2 - i2\gamma_{Lj}\omega}{\omega_{Tj}^2 - \omega^2 - i2\gamma_{Tj}\omega} = \varepsilon_\infty \prod_{j=1}^{N} \left[\frac{\omega_{Lj}^2 - \omega_{Tj}^2 - i2(\gamma_{Lj} - \gamma_{Tj})\omega}{\omega_{Tj}^2 - \omega^2 - i2\gamma_{Tj}\omega} + 1 \right], \quad (2)$$

where ω_{Tj} and ω_{Lj} are the transverse (T), and longitudal (L), frequencies of the polar vibrational mode j, γ_{Tj} and γ_{Lj} are their damping parameters, and ε_∞ is the dielectric constant, caused by the electron polarizability, and a so-called high frequency component of permeability. Expression (2) can be expanded into:

$$\varepsilon(\omega) = \varepsilon_\infty + \varepsilon_\infty \sum_{j=1}^{N} f_j(\omega) + \varepsilon_\infty \frac{1}{2} \sum_{k \neq l}^{N} f_k(\omega) f_l(\omega) + \cdots,$$
$$f_j(\omega) = \frac{S_j \omega_{Tj}^2/\varepsilon_\infty - i2(\gamma_{Lj} - \gamma_{Tj})\omega}{\omega_{Tj}^2 - \omega^2 - i2\gamma_{Tj}\omega}, \quad (3)$$

where $S_j = \varepsilon_\infty(\omega_{Lj}^2 - \omega_{Tj}^2)\omega_{Tj}^2$ is the oscillator strength in the Drude-Lorentz model. Neglecting the damping, or under the condition that the difference between the frequencies of the adjacent oscillators is much larger than their damping parameters, amounts with degrees higher than the first in expression (3) can be omitted, and it will assume the standard form of a multi-oscillator model. For the convenience of a graphic representation of the inputs from individual oscillators, the imaginary part of the dielectric function uses the form of $f_j(\omega)$ that looks like

$$f_j(\omega) = 2\frac{A_j \omega_{Tj}\gamma_{Tj} - i(\gamma_{Lj} - \gamma_{Tj})\omega}{\omega_{Tj}^2 - \omega^2 - i2\gamma_{Tj}\omega}. \quad (4)$$

At the resonant frequency, it is easily seen that $\mathrm{Im}\, f_j(\omega_{Tj}) = A_j$, and that the oscillator strength is connected to this parameter via the expression $S_j = 2\varepsilon_\infty A_j \gamma_{Tj}/\omega_{Tj}$.

For a full analogy to the standard equations, we should also consider the damping parameters of the transverse and longitudal waves to be equal $\gamma_{Tj} = \gamma_{Li}$. However, even without this condition, the additive notation such as (3) is used for describing the optical properties of crystals, which allows us to minimize the quantity of oscillators (independent adjustable parameters) for a good approximation of the experimental spectra.[15]

We chose the model using this exact criterion. In addition, the LST model expresses a significant connection between the adjacent oscillators, especially when the damping is comparable to the difference of the frequencies between them. This often allows us to describe reflectance spectra using a minimal number of oscillators.

Another convenient device for presenting the dielectric functions in the form of expression (2), is the fact that by using the calculated parameters of each separate oscillator $f_j(\omega)$, we can derive the split of the transverse and longitudal frequencies of the optical polar modes (LO-TO):

$$\omega_{Lj}^2 - \omega_{Tj}^2 = 2A_j \omega_{Tj}\gamma_{Tj}. \quad (5)$$

In the additive Drude-Lorentz model, in order to find the splitting of each mode, we must know the ballpark value of its resonant frequency for the real part of its dielectric function, created by all other oscillators. It is this value that must be used as ε_∞ in the expression

$$\omega_{Lj}^2 - \omega_{Tj}^2 = S_j \omega_{Tj}^2/\varepsilon_\infty. \quad (6)$$

Crystal structure and $TbFe_3(BO_3)_4$ vibrational modes

In the ferroborate family, $TbFe_3(BO_3)_4$ refers to those which go through the WPT with a decrease in symmetry from the rhombohedral (spatial group $R32(D_3^7, 155)$, $Z = 1$, formula units in the unit cell) to the trigonal phase ($P3_121$ (D_3^4, 152), $Z = 3$).[16] Later studies with the use of sensitive synchrotron X-ray diffraction technique, allowed to establish a slight deviation from the conventional low-temperature structure.[17] The deviations are weak, and the intensity of prohibited (in the $P3_121$, $Z = 3$) reflections is four orders of magnitude weaker than those that are permitted. According to the authors of Ref. 17, the discrepancy can be eliminated by tripling the volume of the primitive cell with respect to the standard for $P3_121$. In further analysis of the spectra, we will not take this weak distortion into account. Even in using a simplified WPT diagram, the atomic displacement during the transition from $R32$ to $P3_121$ structure, is very small,[16] which should primarily be reflected in the small intensity of the IR and Raman spectral lines, related to the phonons by

the excitations that are ignited at $\mathbf{k} = 0$, during the folding of the Brillouin zone (BZ) in the rhombohedral phase.

In the crystal structure of the given family, it is easy to isolate two types of structural elements. These are the ions of the metals Re^{3+}, Fe^{3+}, and the triangular planar molecules $(BO_3)^{3-}$,[16,18] which can be considered "hard." This representation of the structure is fully justifiable, since the internal vibrations of the BO_3 molecules are sufficiently isolated from the frequency range of the so-called lattice vibrations.[6,19,20]

The theoretical group analysis of the vibrational modes of ferroborates is provided in Ref. 6. Since we are interested only in lattice vibrations, including the translation of Fe^{3+}, Tb^{3+} ions, and the translation and rotation of "hard" triangular planar $(BO_3)^{3-}$ molecules, we will once again provide the results of this analysis for the high-temperature phase (see Table 1).

In the crystal structure, the intermittent layering arrangement of trivalent metal ions Tb^{3+}, Fe^{3+} and $(BO_3)^{3-}$ molecules, is clearly visible (Fig. 1). And, in each of these "layers," (BO_3) and the metals form a triangular lattice with the only difference being that the (BO_3) molecule parameters such as mass, and inertia of the moments, are practically identical, whereas the metals vary greatly in mass. Figure 2 shows a diagram of the distribution of (BO_3) molecules in one of such "layers" within the crystal structure (rhombohedral phase).

The $(BO_3)1$ molecule occupies a high-symmetry position in the lattice, and forms an equilateral triangle made of oxygen ions, with boron at the center. The lattice itself does not have its own dipole moment. The $(BO_3)2$ molecules occupy a position with a local symmetry 2, and can have a dipole moment, as opposed to $(BO_3)1$. The calculation at room temperature according to data from Ref. 16 shows that in $(BO_3)2$, the B^{3+} ion is displaced from the center of gravity of an isosceles oxygen triangle by about 0.05 Å, which, according to the order of magnitude, corresponds to the RMS thermal displacements of atoms in the crystals of many chemical elements at room temperature.[21]

TABLE 1. The symmetry and composition of the vibrational representation of the $TbFe_3(BO_3)_4$ crystal (spatial group $R32$) in the center of the Brillouin zone (Point Γ). The local basis for the displacements t_i, and rotations s_i, of the structural units, is chosen as follows: $z \| c_3$, $x \| c_2$, $y \perp (x,y)$. For positions 32, the x axis is collinear to any of the second order axes, for positions 2, the x axis corresponds to the local axis.

Atom, molecule	Position	Multiple	Type of displacements in the local basis	IR of the factor group
Tb	a (32)	1	t_z	A_2
			t_x, t_z	E
$(BO_3)1$	b (32)	1	t_z	A_2
			t_x, t_y	E
			s_z	A_2
			s_x, s_y	E
Fe	d (2)	3	t_x	$A_1 \oplus E$
			t_x, t_z	$2A_2 \oplus 2E$
$(BO_3)2$	e (2)	3	t_x	$A_1 \oplus E$
			t_y, t_z	$2A_2 \oplus 2E$
			s_x	$A_1 \oplus E$
			s_y, s_z	$2A_2 \oplus 2E$

$\Gamma_{optical} = 3A_1 \oplus 8A_2 \oplus 11E$, $\Gamma_{acoustic} = A_2 \oplus E$

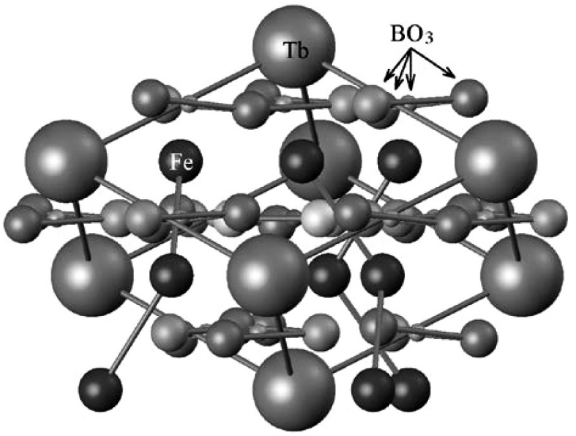

FIG. 1. The structure of $TbFe_3(BO_3)_4$, at room temperature ($R32$ symmetry), according to data from Ref. 16. The c_3 trigonal axis lies in the plane of the drawing.

Figure 2 shows all eight modes, which can be generated by the (BO_3) librations (see Table 1). Further analysis will use the mode number designations adopted in this figure. Table 1 shows that the (BO_3) rotations around the trigonal axis generate $2A_2 \oplus E$-modes, whereas rotations around axes on the basal plane generate $A_1 \oplus A_2 \oplus 3E$-modes.

The A_1(a)-mode does not have a dipole moment. In A_2-modes, the dipole moment is collinear to the trigonal axis, and cannot be generated solely by the rotation of (BO_3) around it. Therefore, two of the three modes of this type, especially A_2(c) and A_2(d), are expected to be weaker in their intensity, than the A_2 (b)-mode, in which the in-phase librations of the $(BO_3)2$ around the axes on the basal plane, can create a significant dipole moment. The reverse scenario is true for E- symmetry modes, the dipole moment of which is perpendicular to the trigonal axis. Of these modes, E(e), E(f), E(h), generated by (BO_3) librations relative to the basal plane axes, are expected to be "weak." Only the E(i) mode, in which the $(BO_3)2$ rotate anti-phase, have a non-vanishing dipole moment.

A feature of point group 32, in which both the factor-groups of the high-temperature and low-temperature $TbFe_3(BO_3)_4$ phases are isomorphic, is that it does not contain elements of mirror symmetry. Its vector representations of axial and polar vectors (rotation and displacement), coincide. Therefore, the drawing in Fig. 2, for libration modes of (BO_3), is equally applicable to the displacement of these same molecules. This means, in particular, that any rotation of the (BO_3) molecule occurs at the same time as a displacement, in the direction that is collinear to the rotation vector. This serves as a "feeding" channel for the amplitude of the oscillating dipole moment for libration modes.

Taking into consideration the aforementioned properties of the crystal structure, the translation modes in the "metal" layer are built in the same way, if the $(BO_3)1$ is replaced by a terbium ion, and $(BO_3)2$ by iron. It should be noted that the modes, in which all atoms of the structure are translated in-phase along one direction, are acoustic and cannot be observed in IR reflectance spectra. Their symmetry is noted in Table 1.

The unity of the crystal class 32 in high- and low-temperature phases, leads to all modes of the high-temperature structure $R32$ being preserved in the low-temperature $P3_121$,

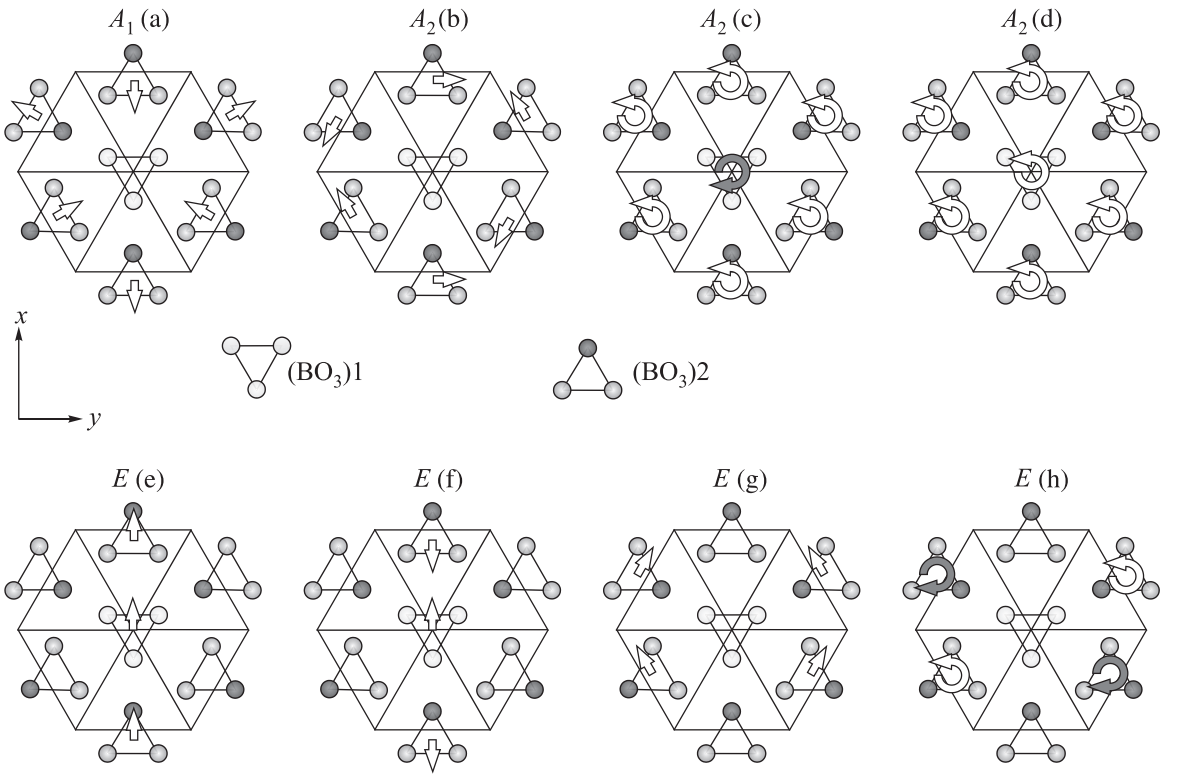

FIG. 2. Diagram of the location of (BO_3) molecules in the $TbFe_3(BO_3)_4$ crystal structure at room temperature.[16] B^{3+} ions are not shown. This is a depiction of (BO_3) libration combinations, that are part of the lattice modes of the crystal. Straight arrows correspond to the directions of the (BO_3) rotation vector, relative to axes located in the *xy* plane. Curved arrows show the direction of rotation, relative to the trigonal axis c_3, which is perpendicular to the plane of the diagram. The *x* axis is collinear with one of the c_2 axes.

without changes in the symmetry, and are converted via the same irreducible representations of the factor-group. Therefore, there are no reasons to expect changes in the polarization selection rules of these modes in Raman and IR spectra. Nor will there be a frequency split of the components of the doubly-degenerate *E*-modes. All modes "occurring" in the low-temperature phase, fall within the spectrum of long-wave excitations as a result of the tripling of the primitive cell volume, i.e., from the boundaries of the high-temperature BZ.

Experimental results and discussion

IR reflectance spectra in the range of lattice vibrations are shown in Fig. 3. As mentioned above, the spectra were recorded in unpolarized light. Therefore, the spectrum formed only by doubly-degenerate polar *E*-modes, was derived using sample No. 1, for the direction of the incident light along the trigonal axis of the crystal (Fig. 3(a)). The dielectric function $\varepsilon_\perp(\nu)$, and the corresponding spectrum of low-frequency excitations, were calculated using these experimental data. Further on, for approximations of the reflectance spectra for sample No. 2 (Fig. 3(b)), $\varepsilon_\perp(\nu)$ was used for the recovery of the dielectric function $\varepsilon_{||}(\nu)$, and the spectra of the A_2- symmetry modes to which it is related, at corresponding temperatures. The imaginary components of the thus obtained $\varepsilon_\perp$ and $\varepsilon_{||}$ functions, are shown in Fig. 4. An example of how the reflectance spectrum of sample No. 2 is calculated at room temperature is illustrated in Fig. 5.

In order to get the best approximation of the experimental reflectance spectra, additional oscillators had to be introduced, that do not fit into the theoretical group calculation of the vibrational modes. In Figs. 5(c) and 5(d) it is possible to discern the wide bands in the frequency regions 200 and 250 cm^{-1}. Their nature is difficult to identify. These can be bands related to, for example, phonon processes of absorption, which can be roughly modeled by the same

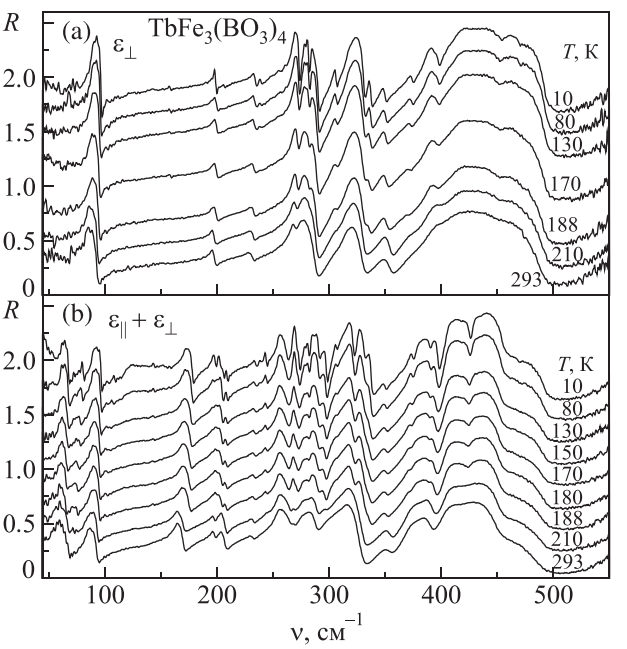

FIG. 3. The temperature evolution of unpolarized reflection spectra $R(\nu)$ of the $TbFe_3(BO_3)_4$ crystal. For sample No. 1 (a), the spectrum is formed only by the dielectric function $\varepsilon_\perp(\nu)$, or by doubly-degenerate polar *E*-symmetry modes. For sample No. 2 (b), the spectrum is the superimposition of reflection spectra formed by $\varepsilon_\perp(\nu)$ and $\varepsilon_{||}(\nu)$. The latter is determined by polar A_2-symmetry modes. The spectra are offset along the vertical axis in increments of 0.2, with decreasing temperature.

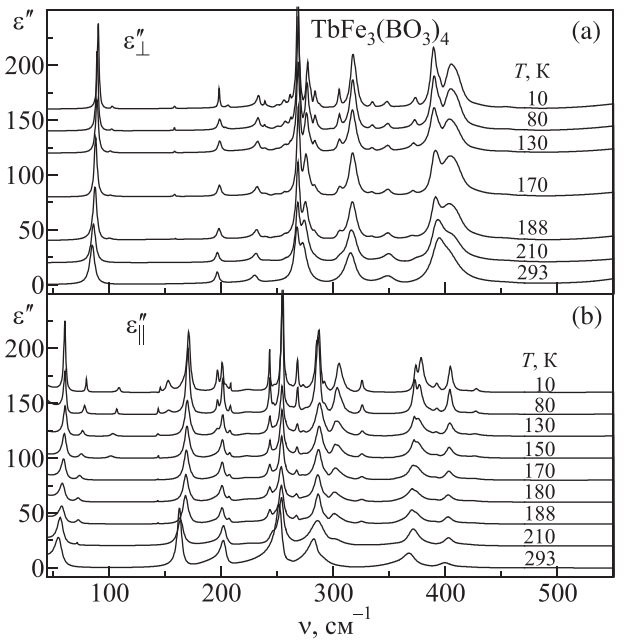

FIG. 4. Temperature evolution of the imaginary components of the dielectric function $\varepsilon_{\perp}(\nu)$ (a), and $\varepsilon_{||}(\nu)$ (b), of the $TbFe_3(BO_3)_4$ crystal, in the frequency range corresponding to the lattice vibrations. The spectra are offset along the vertical axis in increments of 80, with decreasing temperature.

Lorentzians. Another reason for the appearance of wide "excess" bands in adjustable spectra at high temperatures, can be due to transitions between electron levels of the ground multiplet of the rare-earth ion, that has been split in the crystal field. There can also be processes, the physical nature of which is not known to us at the moment.

As a basis for analyzing the vibrational modes, we used oscillators that correspond to pronounced peaks in the imaginary part of the dielectric function, when it is calculated. A significant argument in favor of attributing the band observed in the spectrum to vibrational-type excitation is the

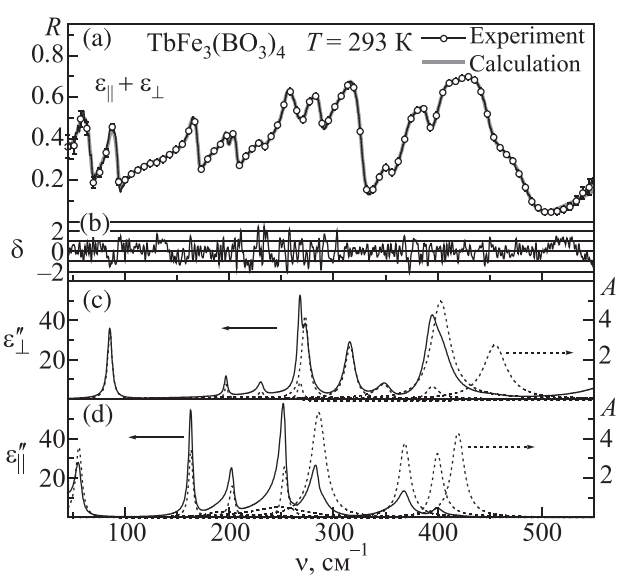

FIG. 5. Experimental and calculated reflectance spectra R, of the $TbFe_3(BO_3)_4$ crystal (sample No. 2) at room temperature, in the frequency range of lattice vibrations (a). The normalized difference, δ, of the experimental and theoretical values of the reflection coefficient (b). The imaginary components of the dielectric functions $\varepsilon_{\perp}(\nu)$ (a), and $\varepsilon_{||}(\nu)$ (solid curves) (c), (d).

specific temperature dependence of a parameter such as damping. Particularly for vibrational excitation, it is typical for this parameter to have less rapid growth when temperature is increased, as opposed to transitions that are of an electron nature.

At low temperatures, the reflectance spectra of sample No. 2 has a wide observable singularity with a maximum in the 120 cm^{-1} region. Its appearance is tied to the fact that at low temperatures, in this frequency range, the imaginary part of the dielectric function responsible for dissipation becomes so small, that the incident electromagnetic wave reaches the opposite surface of the thin sample and can be reflected off of it, and the metal surface of the holder. This circumstance is accounted for in the calculation of the reflection coefficient in formula (1).

Vibrational spectrum of the high-temperature phase

The spectrum of vibrational modes up to 500 cm^{-1}, obtained using the data of IR reflection, contains $8A_2 \oplus 10E$-modes at room temperature. As in, all lattice modes of the A_2-modes are observed, as well as 10 of the 11 possible E-modes. The missing mode at a frequency of 160 cm^{-1} is absent in the IR reflectance spectra, seemingly as a result of its infinitesimally small oscillator strength. It is observable only below WPT. In Raman spectra, this mode is observed confidently[5,6] at all temperatures.

According to the arguments above, this mode's dipole moment's proximity to zero, can serve as evidence in favor of attributing it to the libration of (BO_3). In the low frequency part of the E-mode spectra, at least two polar lines have a small intensity, as opposed to the others. These lines have the frequencies 231 and 268 cm^{-1}. In the spectra of A_2 -symmetry vibration, in this same frequency range, three lines are observed: 163, 203, and 253 cm^{-1} (Fig. 5). It is hard to call them "weak" in comparison to the E-modes, however, because the one with the lowest frequency among them (163 cm^{-1}) has an oscillator strength that is at least twice as big as that of the two others. Within the framework of our qualitative analysis, this spectral line is associated with the A_2-mode (Fig. 2(b)). A complementary mode from the E-symmetry, as far as the nature of the (BO_2) rotations, is E(h). The dipole moment of such a mode in the basal plane really can be infinitesimally small. Another argument in favor of this interpretation is the proximity of the natural frequencies of these modes. Therefore, the lines in the $\varepsilon_{||}$ spectra with frequencies 203 and 253 cm^{-1}, can be attributed to A_2(d)- and A_2(c)-modes. Lines 231 and 268 cm^{-1} in the $\varepsilon_{\perp}$ spectrum can fully correspond to the E(e)- and E(f)-modes. The A_2(c)-mode is complementary to it, and once again the frequency proximity is observed. The mode with the lowest frequency, A_1(181 cm^{-1}), is practically independent of the rare-earth ion substitution in the family ferroborates.[5,6] Within the framework of our classification, this mode has its own displacement vector, like A_1(a) (Fig. 2). Its complementary part can be a mode such as E(e) with a frequency 231 cm^{-1}.

The lines with the lowest frequencies in the $\varepsilon_{||}$ and $\varepsilon_{\perp}$ spectra are 56 and 85.5 cm^{-1}, respectively. They apparently correspond to modes which are mainly generated by vibrations of the rare earth ion. The significant dependence of the

TABLE 2. Relative changes in the coefficient of the quasi-elastic force k, of the low-frequency E-mode in the model, where it is formed by the vibrations of the rare-earth Re ion, relative to the rest of the crystal lattice. M is the mass of the rare-earth ion, ν_T is the frequency of the transverse mode, frequencies from the original paper are in parentheses. See formula (7) and discussion thereof.

Re	M (amu)	ν_T (cm^{-1})	k/k_Y	Δm (amu)	Links
Y	89	102 (107)	1	0	6
Nd	144	89	1.07	30.5	6
Sm[1]	150	83	0.95	−1.5	—
Er	152	79(84)	0.87	−17.5	6
Gd	157	84	1.01	11.3	6
Tb	159	85.5	1.05	22.9	This study
Tb	159	84	1.01	13.3	5

Note: 1—our unpublished data.

frequency of the E-mode in ferroborates, on the mass of the rare-earth ion, can serve as an argument in favor of this interpretation.[5,6*]

This type of vibration can be roughly represented in the form of displacements of the rare-earth ion with mass M, relative to the rest of the lattice. The mass balance is $Fe_3(BO_3)_4$ $m = 403$ amu. The coefficient of the quasi-elastic force k, is expressed in terms of the provided mass and the square of the frequency in a known manner:

$$k_i = \frac{(M_i + \Delta m)(m - \Delta m)}{M_i + m}\nu_i^2. \qquad (7)$$

Here we have to introduce an amendment to the mass Δm, which allows us to consider and evaluate the degree of "dragging" of the mass balance, by the rare-earth ion in this mode. Assuming the same elasticity coefficient, we can evaluate the average value of the correction, $\Delta m \approx 9.8$ amu, i.e., a value sufficiently small in comparison to M and m. In Table 2 we see relative values of the elasticity coefficients for ferroborates with different rare-earth ions. As reference values, data for $YFe_3(BO_3)_4$ are used. For ferroborates Er and Y, there were no pure frequency measurements of the TO modes.[6] However, comparing the data of this study for $TbFe_3(BO_3)_4$ with our data, and the data from the authors of Ref. 5, we can evaluate the overstatement of the given frequencies relative to the ν_T of this mode, approximately within 5 cm^{-1}.

Excitation spectrum of the low-temperature phase

In $TbFe_3(BO_3)_4$, the WPT exhibits properties of a first-order transition, and has a temperature hysteresis at 200–203 K.[22] According to varying literature data, however, bottom and upper bounds of the transition temperature T_s, blur until the range of 192–241 K.[1,3,16,17,23,24] It seems that the value of 241 K, according to data from Ref. 1, is highly exaggerated. First of all, in this study, the crystals were grown without using the latest technology.[8] Second, in Ref. 1, the samples were ceramic compressed tablets, composed, most likely, from fairly small crystallites. In our studies we used the upper boundary of $T_s \approx 203$ K to orient ourselves, and therefore a temperature of 210 K was chosen as being closest to WPT in the high-temperature phase, and 188 K was chosen for the low-temperature phase. Nevertheless, in spite of the fact that in the experiment, the temperature of 210 K was approached from the high-temperature side, the IR reflectance spectrum has impurities from the low-temperature phase (Figs. 3, 4, and 6). When the experiment was conducted, in order to achieve good thermal contact, a thermally conductive adhesive was used to attach the sample to the cold finger cryostat. This could have caused stress across the sample during cooling, by virtue of the difference in thermal expansion coefficients of the copper and the crystal, and possibly, a transition of a part of the sample to the low-temperature phase.

The temperature dependence of the oscillator frequencies, that were used to approximate the experimental reflectance spectra (2), is shown in Fig. 6. As already mentioned, for WPT, as the volume of the primitive cell triples, "new" low-temperature phase modes come from the high-temperature phase of the BZ boundaries. In this case, two scenarios are possible as far as the appearance of such "new" modes.

In the first case, their frequencies are located in the "transparent" regions of the high-temperature spectrum, i.e., outside the reflection bands between ν_T and the ν_L of the polar modes. "New" modes resulting from a weak distortion of the crystal structure during WPT cannot be expected to be intense. This is exactly what is observed in the transparent region (for example, see range 105–265 cm^{-1} in Fig. 6).

Another situation entirely occurs in the second case, wherein the frequency of a "new" mode falls into the reflection band, i.e., the frequency range where the propagation of electromagnetic waves is prohibited within the crystal. It's as though thin "allowed" bands occur within the prohibited band. It can be assumed that as a result of the restructuring of the vibrational spectrum, a formerly prohibited band is divided into two (or possibly, more), new bands with smaller LO-TO splits. In this case, we lose the universality of the thesis of small oscillator strength of the "new" mode, since formally, its oscillator strength, or the LO-TO split, depends on the proportion with which its frequency divided the range of the LO-TO split of the previous mode. From the other side, under resonance conditions, and the situation we are examining is exactly such, even a small stimulating effect can create a large amplitude response.

There exists another point of view,[11] according to which "weak" modes from the high-symmetry phase that fall into the prohibited frequency band, have an inverted sequence for the ν_L and ν_T frequencies. As in, when the dielectric functions are being modeled, they have a negative (!) oscillator strength. This paradox occurs when we make an attempt to form a direct connection between the oscillator strength and the LO-TO split of the mode in the Drude-Lorentz model. Turning to expression (6), it is easy to understand that the value on the right of the denominator, ε_∞, has a negative meaning in the region of the prohibited band, which gives rise to the inversion being discussed.

The LST model used by us from this point of view is universal, since expression (2), is completely indifferent to the numbering of poles (ν_T) and zeroes (ν_L) and they can be combined in order to express the parameters of the individual Lorentzians (4), at random. The obtained oscillators can

*Data for the A_2-modes are currently unknown to the authors.

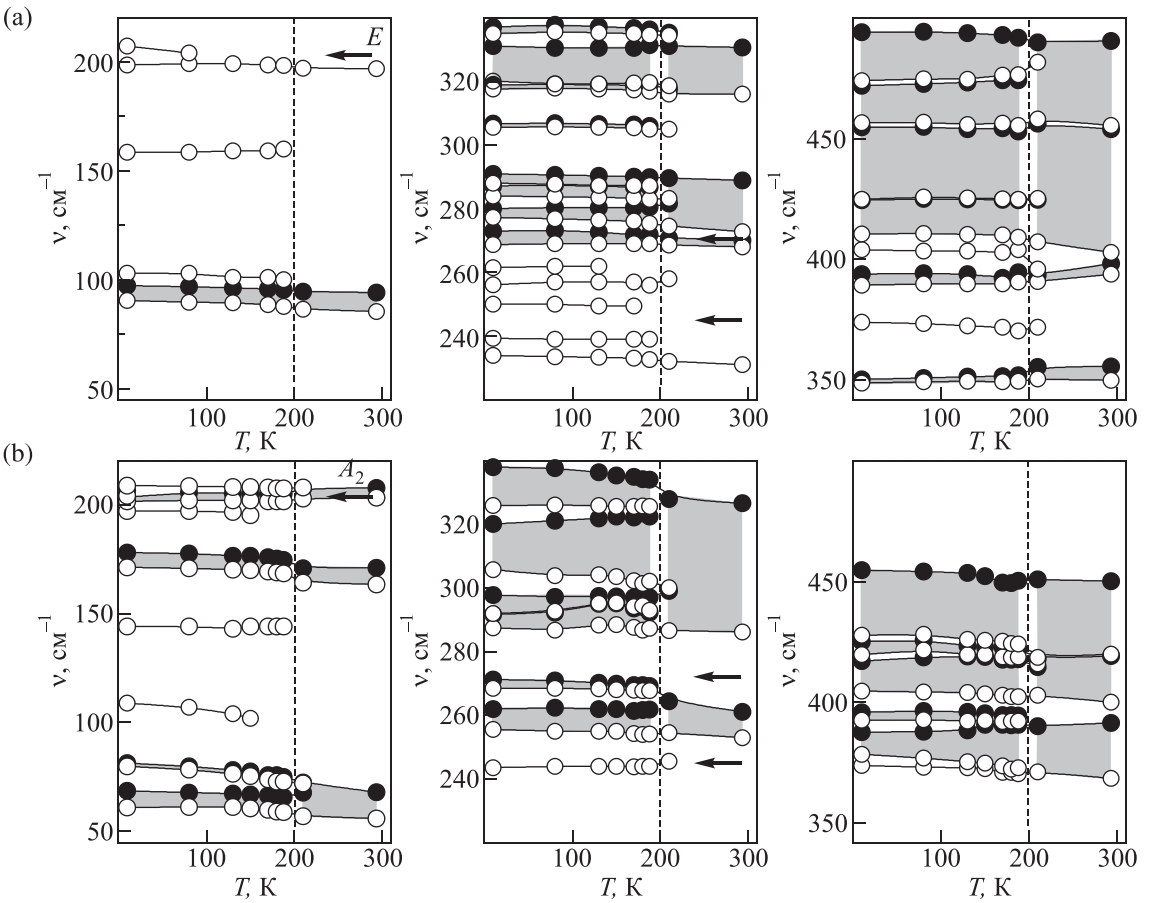

FIG. 6. Temperature dependences of TO (○) and LO (●) frequencies of the symmetry modes E (a) and A_2 (b) of the $TbFe_3(BO_3)_4$ crystal. Grey areas show LO-TO splits for the modes in which this parameter is greater than 1 cm^{-1}. Horizontal arrows indicate frequencies at which, for a temperature 10 K, there is an observable dependence of the reflectance spectrum, on the external magnetic field, as it is applied along the trigonal axis of the crystal. Dotted lines correspond to the WPT temperature.

have negative and positive strengths, and the model dielectric function will remain unchanged. From our point of view, the most physically justifiable restriction on the correspondence between the poles and the zeroes of the dielectric function (parameters of the individual oscillators) is proposed by T. Kurosawa. This restriction does not allow for an intersection of the prohibited frequency range of one mode, with another.

The situation described above is actualized during a transition of $TbFe_3(BO_3)_4$ to the low-temperature phase, in broad reflection bands of the A_2-symmetry mode, with frequencies of 286, 400, 420 cm^{-1}, and E-symmetries of 273, 403, and 456 cm^{-1} (Fig. 6).

The frequencies of the modes active in the IR absorption for high-temperature and low-temperature phases of $TbFe_3(BO_3)_4$, are shown in Tables 3 and 4. It should be noted that with decreasing temperature in the reflectance spectrum, weak lines are observed, that are difficult or impossible to distinguish at a temperature of 188 K, which is directly below T_S. They include the excitation of the E-symmetry with frequencies of 207, 250, and 261 cm^{-1} and A_2-symmetries with frequencies of 109, 153, 107, and 204 cm^{-1}.

A_2-modes 109, 197 cm^{-1}, and E-modes 250, 261 cm^{-1}, have a weak intensity, but are well-enough fixed in the reflectance spectrum at temperatures below 150 K (Figs. 3, 4, and 6), as their damping parameters decrease. The A_2-modes 153, 204 cm^{-1}, and E-mode 207 cm^{-1}, are visible only at low temperatures. In this case, the width of the absorption line 153 cm^{-1}, is much greater than the width of the adjacent phonon origination lines. The nature of this excitation (or the peak in the imaginary component of the dielectric function), observable in the spectrum of A_2-modes, remains unknown. In our opinion, modes 204 and 207 cm^{-1} can be related to the electron transitions between the levels of the ground Tb^{3+} ($^7F_6$) multiplet, split in the crystal field. The reflectance spectrum reaction to the application of an external magnetic field can serve as basis for this conclusion[**] (Fig. 7). The magnetic field also affects the shape of the reflectance spectrum at frequencies 245 and 271 cm^{-1}, although to a much lesser degree (Fig. 7). Modes 250, 269 cm^{-1} of the E-symmetry, and modes 244, 268 cm^{-1} of the A_2-symmetry, are located near these frequencies. Of these, the most likely candidate for having electron origin can be the 250 cm^{-1} mode, since it demonstrates a sufficiently rapid broadening during temperature increase.

In the terbium ferroborate, the energy levels of the ground multiplet are established using thermally stimulated processes in the absorption spectra, for the transitions from $^7F_6 \rightarrow {}^7F_3$.[25] The calculation of the parameters of the crystal field, conducted in this study, allows us to evaluate the frequencies of possible transitions at low temperatures in the

[**]In the Raman spectra,[5] line 208 cm^{-1} undergoes the most significant frequency shift in the magnetic field.

TABLE 3. Frequencies of *E*-symmetry modes in cm^{-1}, observable in the $TbFe_3(BO_3)_4$ crystal, according to this study, as well as Raman data.[5] The top line shows the temperature in Kelvin. The TO and LO symbols designate frequencies of the transverse and longitudal waves, respectively.

2 (Ref. 5)		10		188		293		293 (Ref. 5)	
TO	LO	TO	LO	TO	LO	TO	LO	TO	LO
89.1	97.0	90.6	97.2	87.8	95.4	85.5	94	84.2	93.6
		103	103.1	100	100				
114.5									
158.5		158.5	158.6	160	160	—	—	159.9	
169.5									
191.4									
195.7									
199.0	199.8	198.5	199.4	198.3	199.7	196.8	198.1	197.1	198.3
208.1		207	207.1						
235.0		233.9	234.8	232.6	233.6	231	232.2	230.4	
		239.3	239.4	239	239.1				
		250	250.1						
256		256.2	256.3	256	256				
		261.5	261.6						
274.0		268.7	273	269	272	268	270.1	269.4	
278.1		277.3	280.1	275.5	280.5	272.8	288.9	273.5	289
		280.7	282.3	280.8	281.7				
283.6		284	287.2	283	286.8				
	291.3	288	290.9	287.3	289.9				
306		305.6	306.7	305	306				
307.5									
312.4									
318.4		317.6	319	317	319.1	316	330.7	315.4	330.4
	332.1	320.1	331.2	319.7	331.5				
338.6		335	337.1	334.6	336.3				
349.3	351.5	348.8	350.5	349.7	352.2	350	355.8	350.7	355.8
368.5									
375.1		374.1	375	370.5	371				
396.1		389.4	394	390.8	394.7	394	398.4	394.2	
398.9									
403.5		404	406.6	404	406.4				
		410.5	424.6	409.2	424.5	403	454	445	
450.3		424.9	454.8	424.9	453				
470		456.7	471.9	455.4	474.3	455.5	490.5	489	
492.0		474	494	476.5	491.8				

discussed ranges: 200 and 206 cm^{-1} (Γ_3), 218 cm^{-1} (Γ_1 or Γ_2), 236 and 259 cm^{-1} (Γ_3). At 100 K, transitions corresponding to excitation energies of electron levels 196, 225, and 247 cm^{-1}, were experimentally observed in Ref. 25. The symmetry of the transitions described above, is in the vicinity of the trigonal crystal field. In the low-temperature phase, the local field in the position of the rare-earth ion, decreases until it becomes monoclinic, which can create a disruption in the polarization selection rules. This splitting of the ground multiplet of the Tb^{3+} ion, with similar electron level energies, is observed in isostructural alyumoborate $TbAl_3(BO_3)_4$.[26,27]

Comparison with Raman data

As seen in Tables 3 and 4, for the high temperature phase of the $TbFe_3(BO_3)_4$ crystal, the data on the frequency of vibrational modes from this study, and the Raman results,[5] coincide fairly well. In the region of the spectrum up to 400 cm^{-1}, where adjacent modes have a large separation of frequencies (in comparison to their LO-TO split), the match-up is almost complete for both *E*- and A_2-modes, which are observable in the Raman spectrum thanks to the Pockels effect. Specifically, that the A_2-modes in Raman spectra appear only in a "mixed" state, i.e., with wave vector directions which are neither purely longitudinal nor transverse.[28] In these directions, the frequency at which the mode is observed within the spectrum, obtains an interim value between ν_T and ν_L. This is fulfilled for all A_2-modes from Ref. 5, except for the lines with frequencies of 277 and 470 cm^{-1} (see Table 4). It is not uncommon for a mode to be clearly seen in the Raman spectrum, without appearing in IR (and vice versa). The *E*- 160 cm^{-1} mode can be used as an example (Table 3). In the case of A_2-modes, this situation is impossible, since according to their origin, their Raman activity is directly proportional to the dipole moment, and consequently, can only be observed for the spectral lines of intense IR absorption (having a large oscillator strength). In addition, for those wave vector directions, in which the A_2-modes can be observed in the Raman spectrum, one of the components of doubly-degenerate *E*-symmetry modes also has a "mixed" character, and can interact with A_2, if they fall in the same frequency interval.[28] Therefore, we believe that the above-mentioned modes of 277 and 470 cm^{-1}, are more likely to be related to *E*-symmetry modes. The first of them

TABLE 4. Frequencies of the A_2-symmetry mode, observable in the $TbFe_3(BO_3)_4$ crystal, according to this study, as well as Raman data.[5] Designations same as in Table 3.

10		188		293		293 (Ref. 5)
TO	LO	TO	LO	TO	LO	
61	68.7	59	65.7	56	68	60.5
80	81.3	73	75			
109	109.4					
144	144.3	144	144.1			
153	154.4					
171.2	177.8	168.4	174.4	163.2	170.9	
197	198					
201.3	203.2	201.3	204.7	203	207.6	205.4
204	206.3					
208.6	209.2	207.4	208.6			
243.5	244.5	243.9	244.7			
255.5	262	254.1	261.8	252.9	261	258.5
268.4	271.2	267.8	269.2			
						277.2
287.5	291.7	287.3	292.3	286.2	326.7	301.4
291.9	297.8	293	297			
305.7	320.1	302.2	322.5			
325.9	338	325.6	334			
374	375.2	370.5	371.1			
378.4	387.6	372.9	390.8	368.6	391.4	372.6
392.6	395.8	392.2	394.5			
404.6	417.1	402.4	417.9	400	419.1	
419.7	425.2	418.8	422			
427.8	454.8	424.1	450.4	419.9	450.1	
						470

falls within the range of the LO-TO split for the mode 273 cm^{-1}, and the high-frequency falls within the mode 456 cm^{-1} (see Table 3).

A similar pattern of interaction for A_2- and E- modes is observed, it would seem, for Raman lines 445 cm^{-1}.[5] From one side, this frequency falls within the range of the LO-TO split of the E-mode (403–454 cm^{-1}). From the other, in Raman spectra, the position of this line is practically independent of the direction of the wave vector, as though the corresponding mode has no dipole moment. If we also take into account the fact that the line is located in the range of the LO-TO split of the A_2-mode (420–450 cm^{-1}), at wave vector lengths that are realized in the Raman experiment,[5] then we can have a situation in which there is virtually no angular frequency dispersion. This scenario is observable for some polar modes in Raman spectra of crystalline quartz.[28]

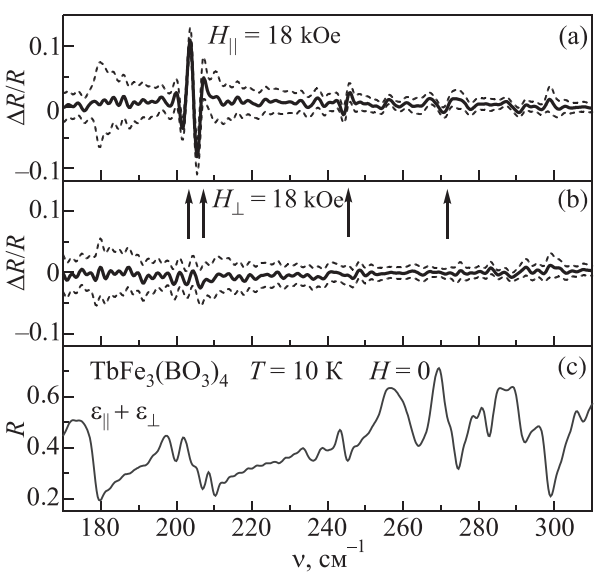

FIG. 7. The plot of the relative differential reflectance spectrum of sample No. 2 of the $TbFe_3(BO_3)_4$ crystal, upon application of an external magnetic field with a strength of 18 kOe, along (a), and perpendicular (b) to, the trigonal axis at a temperature of 10 K. The reflectance spectrum in a zero field (c). Dotted lines show the confidence interval, associated with statistical measurement errors. Vertical arrows indicate the frequencies at which the reflectance spectrum has a field dependence.

Conclusion

In the spectra of the high-temperature phase $R32$, for the $TbFe_3(BO_3)_4$ crystal, all lattice polar modes $8A_2 \oplus 11E$ are detected. Based on a qualitative analysis of the types of motion of the crystal structure components in vibrational modes, they are conditionally matched to nine lines of the experimental IR reflectance spectrum.

In the low-temperature phase $P3_121$, close to T_s we observe 19 of the 20 A_2-modes predicted by the theoretical group analysis. At low temperatures, the number of observable lines increases to 23. One of the excess lines (153 cm^{-1}) is characterized by a large damping parameter, and is not identified in this study. The line with the frequency 204 cm^{-1}, most likely has an electron origin. Another one of the excess lines at 197 cm^{-1}, also appears to have an electron nature. Further detailed studies are necessary, in order to clarify these assumptions.

According to IR reflectance data, in the $\varepsilon_\perp$ spectrum of the low-temperature phase, 27 lines are observed, of which two, 207 and 250 cm^{-1}, are most likely related to electron transitions. Therefore, taking into account the Raman data[5] in the low-temperature spectrum of the lattice vibrations of $TbFe_3(BO_3)_4$, 33 of 35 E-symmetry modes allowable by group theoretical analysis,[16] are detected.

In conclusion, the authors would like to express their gratitude to A. V. Peschanskiy and V. A. Bedarev for kindly providing the research samples.

[a)]Email: kurnosov@ilt.kharkov.ua

[1]Y. Hinatsu, Y. Doi, K. Ito, M. Wakeshima, and A. Alemi, J. Solid State Chem. **172**, 438 (2003).
[2]A. M. Kadomtseva, U. F. Popov, G. P. Vorobyev, A. P. Pyatakov, S. S. Krotov, K. I. Kamilov, V. U. Ivanov, A. A. Muhin, A. K. Zvezdin, A. M. Kuzmenko, L. N. Bezmaternykh, I. A. Gudim, and V. L. Temerov, Fiz. Nizk. Temp. **36**, 640 (2010) [Low Temp. Phys. **36**, 511 (2010)].
[3]M. N. Popova, J. Magn. Magn. Mater. **321**, 716 (2009).
[4]A. N. Vasilyev and E. A. Popova, Fiz. Nizk. Temp. **32**, 968 (2006) [Low Temp. Phys. **32**, 735 (2006)].
[5]A. V. Peschanskiy, A. V. Eremenko, V. I. Fomin, L. N. Bezmaternykh, and I. A. Gudim, Fiz. Nizk. Temp. **40**, 219 (2014) [Low Temp. Phys. **40**, 171 (2014)].
[6]D. Fausti, A. A. Nugroho, P. H. M. van Loosdrecht, S. A. Klimin, M. N. Popova, and L. N. Bezmaternykh, Phys. Rev. B **74**, 024403 (2006).
[7]U. Adem, L. Wang, D. Fausti, W. Schottenhamel, P. H. M. van Loosdrecht, A. Vasiliev, L. N. Bezmaternykh, B. Büchner, C. Hess, and R. Klingeler, Phys. Rev. B **82**, 064406 (2010).
[8]L. N. Bezmaternykh, V. L. Temerov, I. A. Gudim, and N. A. Stolbovaya, Crystallogr. Rep. **50**(S1), S97 (2005).
[9]J. A. Stratton, *Electromagentic Theory* (OGIZ, Moscow, Leningrad, 1948) [Julius Adams Stratton, *Electro-Magnetic Theory* (McGraw-Hill Book Company, New York, London, 1941)].
[10]V. Železný, E. Cockayne, J. Petzelt, M. F. Limonov, D. E. Usvyat, V. V. Lemanov, and A. A. Volkov, Phys. Rev. B **66**, 224303 (2002).

[11]G. A. Komandin, A. A. Volkov, O. E. Porodinkov, I. E. Spektor, and S. V. Chuchupal, Fiz. Tverd. Tela **55**, 1147 (2013).
[12]T. Kurosawa, J. Phys. Soc. Jpn. **16**, 1298 (1961).
[13]A. S. Barker, Jr., Phys. Rev. **136**, A1290 (1964).
[14]D. W. Berreman and F. C. Unterwald, Phys. Rev. **174**, 791 (1968).
[15]A. Deinega and S. John, Opt. Lett. **37**, 112 (2012).
[16]C. Ritter, A. Balaev, A. Vorotynov, G. Petrakovskiĭ, D. Velikanov, V. Temerov, and I. Gudim, J. Phys.: Condens. Matter **19**, 196227 (2007).
[17]J. E. Hamann-Borrero, M. Philipp, O. Kataeva, M. V. Zimmermann, J. Geck, R. Klingeler, A. Vasiliev, L. Bezmaternykh, B. Büchner, and C. Hess, Phys. Rev. B **82**, 094411 (2010).
[18]S. A. Klimin, D. Fausti, A. Meetsma, L. N. Bezmaternykh, P. H. M. van Loosdrecht, and T. T. M. Palstra, Acta Crystallogr., Sect. B: Struct. Sci. **61**, 481 (2005).
[19]G. Barros, E. N. Silva, A. P. Ayala, I. Guedes, C.-K. Loong, J. Wang, X. Huc, and H. Zhang, Vib. Spectrosc. **46**, 100 (2008).
[20]H. R. Xia, L. X. Li, J. Y. Wang, W. T. Yu, and P. Yang, J. Raman Spectrosc. **30**, 557 (1999).
[21]D. S. Gemmell, Rev. Mod. Phys. **46**, 129 (1974).
[22]G. A. Zvyagina, K. R. Zhekov, L. N. Bezmaternykh, I. A. Gudim, I. V. Bilych, and A. A. Zvyagin, Fiz. Nizk. Temp. **34**, 1142 (2008) [Low Temp. Phys. **34**, 901 (2008)].
[23]A. N. Vasiliev, E. A. Popova, I. A. Gugim, L. N. Bezmaternykh, and Z. Hiroi, J. Magn. Magn. Mater. **300**, E382 (2006).
[24]A. M. Kuzmenko, A. A. Muhin, V. U. Ivanov, A. M. Kadomtseva, S. P. Lebedev, and L. N. Bezmaternykh, JETP **140**, 131 (2011).
[25]M. N. Popova, T. N. Stanislavchuk, B. Z. Malkin, and L. N. Bezmaternykh, J. Phys.: Condens. Matter **24**, 196002 (2012).
[26]I. Couwenberg, K. Binnemans, H. De Leebeeck, and C. Görller-Walrand, J. Alloys Compd. **274**, 157 (1998).
[27]A. M. Kadomtseva, Yu. F. Popov, G. P. Vorob'ev, N. V. Kostyuchenko, A. I. Popov, A. A. Mukhin, V. Yu. Ivanov, L. N. Bezmaternykh, I. A. Gudim, V. L. Temerov, A. P. Pyatakov, and A. K. Zvezdin, Phys. Rev. B **89**, 014418 (2014).
[28]S. M. Shapiro and J. D. Axe, Phys. Rev. B **6**, 2420 (1972).

Translated by A. Bronskaya